Regulation of oxytocin-induced calcium transients and gene expression in engineered myometrial tissues by tissue architecture and matrix rigidity

Antonina P. Maxey [a], Jaya M. Travis [a], Megan L. McCain [a,b,*]

[a] *Laboratory for Living Systems Engineering, Alfred E. Mann Department of Biomedical Engineering, USC Viterbi School of Engineering, University of Southern California, Los Angeles, CA, USA*
[b] *Department of Stem Cell Biology and Regenerative Medicine, Keck School of Medicine of USC, University of Southern California, Los Angeles, CA, USA*

ABSTRACT

The uterus is susceptible to benign tumors known as fibroids, which have been associated with many pregnancy complications, including preterm labor. However, the impact of fibrotic tissue remodeling on the physiology of the myometrium, the smooth muscle layer of the uterus, is poorly understood, in large part due to a lack of model systems. In this study, we engineered healthy-like and fibrotic-like myometrium by culturing human myometrial smooth muscle cells on polyacrylamide hydrogels micropatterned with fibronectin to independently tune matrix rigidity and tissue alignment, respectively. We then evaluated calcium transients in response to oxytocin stimulation. Isotropic myometrial tissues on stiff substrates (representing fibrotic myometrium) had shorter calcium transients due to shorter decay time compared to aligned myometrial tissues on soft substrates (representing healthy myometrium). Calcium transients in aligned tissues had longer response times and longer decay times than isotropic tissues, irrespective of substrate stiffness. The amplitude of calcium transients was also higher on soft substrates compared to stiff substrates, irrespective of tissue alignment. We also performed RNA sequencing to detect differentially expressed genes between healthy- and fibrotic-like tissues, which revealed that a bitter taste receptor shown to induce smooth muscle relaxation, *TAS2R31,* was down-regulated in fibrotic-like tissues. Finally, we measured oxytocin-induced calcium transients in response to pre-treatment with progesterone, caffeine, thrombin, and nifedipine to demonstrate applications for our model system in drug screening. Both progesterone and caffeine caused a decrease in calcium transient duration, as expected, while thrombin and nifedipine had less impact. Collectively, our engineered model of the myometrium enables new insights into myometrial mechanobiology and can be extended to identify or screen novel drug targets.

1. Introduction

Uterine contractions are generated by the smooth muscle cells in the middle layer of the uterus, known as the myometrium. Healthy myometrium consists of circularly or longitudinally aligned muscle layers (Wray and Prendergast, 2019; Flake et al., 2018) with an elastic modulus of 10–30 kPa (Omari et al., 2015; Acar et al., 2016), depending on the measurement technique. Fibrotic regions or fibroids are prevalent in 4.5–68.6% of women (Marsh et al., 2018) and are associated with abnormal uterine contractions in non-pregnant women, which may contribute to infertility (Nishino et al., 2005). Uterine fibroids also affect 2–10% of pregnant women (Spyropoulou et al., 2020) and have been associated with complications such as preterm labor (Landman et al.,

2022) and Caesarean section (Acar et al., 2016; Parazzini et al., 2016). Structural evaluation of the extracellular matrix (ECM) in fibroids has shown random orientations of collagen fibrils (Leppert et al., 2006) and a two to four-fold increase in tissue stiffness (Acar et al., 2016; Jayes et al., 2019), which may contribute to preterm labor by reducing the distension threshold required to initiate labor or causing ill-timed contractions (Rizk et al., 2021). Preterm labor, defined as labor that begins prior to 37 weeks of gestation, almost always leads to preterm birth, the leading cause of neonate death (Simhan, 2010). Current interventions for preterm labor are limited and include administration of tocolytics, a class of drugs that temporarily delay labor (Haas et al., 2014). However, most tocolytics, such as nifedipine, a beta-2 adrenergic receptor agonist, are non-specific and can cause many adverse side effects for both the

mother and fetus (Arrowsmith et al., 2010; Lamont et al., 2016; Kim et al., 2019). Fibroids can also decrease the force of contractions or disrupt the coordination between cells, resulting in dysfunctional labor (Rizk et al., 2021), Caesarean section (Zhang et al., 2007), or postpartum hemorrhage (Oyelese and Ananth, 2010). Caesarean sections also cause uterine scarring and increased matrix deposition, which can result in dysmenorrhea for non-pregnant women (Ewies and Zanetto, 2017) and increase the risk for preterm labor in future pregnancies (Williams et al., 2021). The overall impact of fibroids on childbirth is likely to increase because fibroid incidence increases with age (Lou et al., 2023) and the median age of childbirth increased by three years between 1990 and 2019 (Morse, 2022). Thus, there is a significant clinical need to better understand relationships between fibrosis and myometrial smooth muscle cell physiology.

Although studies have shown that substrate stiffness modulates contractile phenotypes in airway smooth muscle cells (Polio et al., 2019), the impact of matrix stiffness on myometrial smooth muscle cells remains poorly understood. This is partly due to a lack of model systems, which are generally limited to: animal models (mostly rodents) that are fundamentally incapable of recapitulating many unique features of human parturition (Mitchell and Taggart, 2009); or explanted human tissue strips collected during elective Caesarean sections, which are rare, difficult to prepare and maintain, and suffer from low reproducibility (Arrowsmith et al., 2018). Human *in vitro* models, which are relatively accessible and reproducible, have also been generated by culturing human myometrial smooth muscle cells as a monolayer or engineered tissue ring (Souza et al., 2017). However, evaluating the physiological effects of fibrotic-like conditions on human myometrial cells in a controlled *in vitro* setting has not yet been attempted.

To address these knowledge gaps in myometrial mechanobiology, our goal was to engineer an *in vitro* system for directly measuring the effects of tissue architecture and matrix rigidity on the structure, physiology, and transcriptome of human myometrium. To mimic healthy and fibrotic myometrium, we adapted our previous techniques (Ariyasinghe et al., 2017) for microcontact printing fibronectin onto polyacrylamide hydrogels to garner independent control over tissue alignment and matrix rigidity. We then cultured primary human myometrial smooth muscle cells on these hydrogels and characterized tissue structure and identified differentially expressed genes via RNA sequencing. We also evaluated calcium transient morphology in response to oxytocin stimulation, revealing unique effects of matrix rigidity and tissue alignment on calcium dynamics. Lastly, we evaluated the effects of several compounds, including nifedipine, on oxytocin-induced calcium transients to serve as a proof-of-concept demonstration of our assay for applications in compound screening. Collectively, our engineered model of the myometrium enables new insights into myometrial mechanobiology and can also be used to identify novel drug targets and screen the functional effects of compounds.

2. Methods

2.1. Substrate preparation

Polyacrylamide hydrogels were fabricated according to previous methods (Rexius-Hall et al., 2021; McCain et al., 2012). Briefly, solutions of 40% acrylamide (Bio-Rad) and 2% N, N′-methylenebisacrylamide (Sigma-Aldrich) were combined with water, ammonium persulfate, and TEMED using indicated ratios for 13 kPa or 90 kPa elastic modulus. The solution was combined with streptavidin acrylamide (1:6 dilution), then 20 μL of the resulting solution was pipetted onto 25 mm glass coverslips activated with sodium hydroxide, APTES, and glutaraldehyde (Rexius-Hall et al., 2021). Non-activated 18 mm glass coverslips were placed atop the solution to flatten the polyacrylamide drop. The hydrogels were cured at room temperature for 30 min, then the non-activated 18 mm coverslips were removed under sterile conditions using a razor blade. Cured hydrogels were rinsed three

times with PBS then stored at 4 °C in PBS for up to one week.

Hydrogels were microcontact printed with biotinylated fibronectin in either aligned or isotropic patterns per previously described methods (Rexius-Hall et al., 2021; Desai et al., 2014) (Fig. 1A). Polydimethylsiloxane (PDMS) stamps were cast on wafer templates prepared using standard photolithography (Qin et al., 2010). Wafer templates were either un-patterned (for isotropic) or patterned with 40 μm wide rows separated by 75 μm wide gaps (for aligned). Biotinylated fibronectin was prepared by incubating sulfo-NHS-LC-biotin (Thermo), fibronectin (Corning), and sodium carbonate overnight, then dialyzing against PBS to remove un-reacted biotin, similar to previously published protocols (McCain et al., 2012). Feature-less PDMS stamps were submerged in 95% ethanol, sonicated for 30 min, dried with compressed air under sterile conditions, coated with biotinylated fibronectin, and incubated for at least 1 h. Simultaneously, polyacrylamide hydrogels were dried for 30 min in a desktop incubator at 37 °C. Excess fibronectin was removed from the PDMS stamps, then stamps were dried with compressed air. For isotropic samples, the dried PDMS stamps were placed directly on the dried polyacrylamide hydrogels with light pressure. For aligned samples, a UVO-treated (8 min) lane template stamp was used to selectively remove biotinylated fibronectin from a flat PDMS stamp, resulting in 40 μm wide lanes; the flat PDMS stamp was then placed onto the polyacrylamide hydrogel with light pressure. Stamps remained in contact with the gel for approximately 6 min before the stamp was removed and the coverslip was rinsed three times with PBS. Microcontact printed hydrogels were stored at 4 °C then seeded within hours of stamping.

2.2. Cell culture

Cell culture media was prepared by combining vascular cell basal medium (ATCC PCS-100-030), vascular smooth muscle cell growth kit (ATCC PCS-100-042), and penicillin-streptomycin (0.1%) and then sterilizing with a 0.22 μm vacuum filter. Primary human uterine smooth muscle cells (HUtSMC, ATCC PCS-460-011) were received at passage two (batch #62232441) and stored in liquid nitrogen. T75 flasks were coated with 0.1% gelatin (Stem Cell Technologies) at 37 °C for 30 min, followed by incubation with warm media for an additional 30 min. The cell vial was then thawed in a water bath, resuspended in warm media, and divided between three gelatin-coated T75 flasks. Cells were maintained at 37 °C, 5% CO$_2$ and media was replenished after two days. Cells were passaged using trypsin on the third day (approximately 75% confluence) into nine T75 gelatin-coated flasks. On the fifth day, cells were passaged, resuspended in freezing media (media supplemented with 10% FBS and 10% DMSO), distributed into cryovials, and cryopreserved in liquid nitrogen. For experiments, a single cryovial was similarly thawed and expanded in gelatin-coated T75 flasks. Cells were then detached from flasks and seeded at a density of 125,000 cells per 2 mL media on microcontact-printed polyacrylamide hydrogel coverslips in a 6-well plate. All measurements were collected within four days of seeding at passage five.

2.3. Immunochemistry and structural quantification

After two days of culture, coverslips were rinsed with PBS and fixed and permeabilized with paraformaldehyde (4%) and Triton (0.1%), respectively, for 10 min. Coverslips were then rinsed three times with PBS and stored at 4 °C for a maximum of one week.

Primary staining was performed by inverting coverslips on droplets of PBS with anti-fibronectin antibody produced in rabbit (Sigma, 1:200) for 1.5 h followed by three PBS rinses. For secondary staining, coverslips were incubated with goat anti-rabbit antibody conjugated to Alexa Fluor 546 (Life Technologies, 1:200), DAPI (1:200), and phalloidin conjugated to Alexa Fluor 488 (Life Technologies, 1:200) for 1.5 h. Coverslips were then rinsed three times with PBS, slightly dried, inverted onto 30 μL of ProLong Gold Antifade (Life Technologies) on a glass slide, and sealed
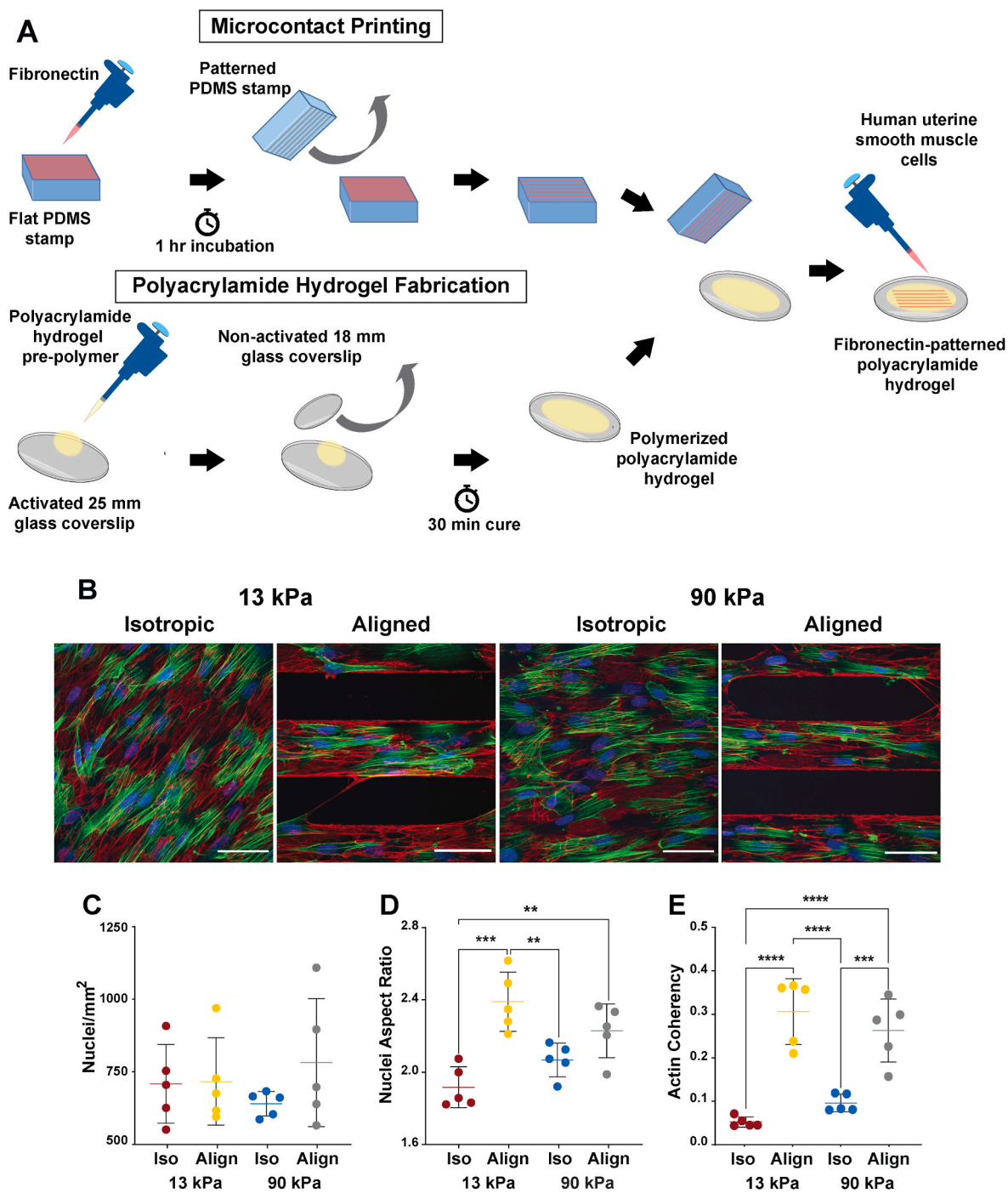
Fig. 1. Structure of engineered myometrial tissues. (A) Schematic of microcontact printing and polyacrylamide hydrogel fabrication. (B) Representative fluorescent images of myometrial tissues on isotropic or aligned fibronectin micropatterns on 13 kPa or 90 kPa polyacrylamide gels. Blue: nuclei, green: F-actin, red: fibronectin. Scale bar: 50 μm. (C) Number of nuclei normalized to fibronectin area in field of view. (D) Nuclei length divided by width (aspect ratio). (E) Actin alignment quantified as coherency. * denotes p < 0.05, ** p < 0.01, *** p <0.001, **** p < 0.0001 using Tukey's multiple comparisons test. (For interpretation of the references to colour in this figure legend, the reader is referred to the Web version of this article.)

with nail polish.

Samples were imaged with a Nikon C2 point-scanning confocal fluorescent microscope with a 60x oil (NA=1.515) objective with a minimum of five fields of view per coverslip. For each coverslip, actin coherency was quantified using the phalloidin stain and the ImageJ plugin, OrientationJ (Fonck et al., 2009). Five fields of view per coverslip were stitched together and coherency was calculated for the stitched image. To calculate cell density, the number of nuclei in each field of view (based on the DAPI stain) was quantified and averaged using

CellProfiler and then divided by an estimate of the fibronectin surface area coverage. CellProfiler was also used to measure the average major and minor axes and aspect ratio of the nuclei for each coverslip. Each datapoint represents one coverslip, with a total n=5 coverslips. All data was statistically compared with one-way ANOVA, Dunnet's or Tukey's multiple comparisons test in Graphpad Prism.

2.4. Live imaging and analysis of calcium transients

Oxytocin powder (Sigma Aldrich) was reconstituted with PBS and stored at $-20\,°C$ in 2 ug/uL stock aliquots. Immediately before experiments, aliquots were warmed and added to Tyrode's solution (5.0 mM HEPES, 1.0 mM magnesium chloride, 5.4 mM potassium chloride, 135.0 mM sodium chloride, 0.33 mM potassium phosphate, 1.8 mM calcium chloride, 5.0 mM D-glucose, pH 7.4 at $37\,°C$).

Fluo-4 AM calcium-sensitive dye (Invitrogen) was reconstituted in Pluronic-127, added to media for a final concentration of 1.7 µg/mL, then added to a coverslip well to incubate for 40 min. Samples were then rinsed with $37\,°C$ Tyrode's solution three times to remove unincorporated Fluo-4, then placed in the $37\,°C$ microscope incubation chamber with 1 mL Tyrode's solution to acclimate for 10 min prior to experiments.

Fluo-4 fluorescence intensity and brightfield images were collected over the course of 3 min using a 20x objective lens and an Andor Zyla sCMOS camera at two frames per second. Oxytocin solutions (0.001, 0.01, 0.1, 1 g/L) were added at the 50 s timepoint. Drug response studies followed a similar protocol while also adding the drug prior to oxytocin. Incubation times for each drug were based on previous studies and varied by drug to account for mechanism of action. Progesterone (5 µg/mL) was added 24–36 h before calcium imaging. Caffeine (5 mM) (Burghardt et al., 1999) and thrombin (1 U/mL) (Nishimura et al., 2020) were added to the Tyrode's at the start of the chamber acclimation for a total of 15 min before imaging. Nifedipine (5 µg/mL) was added to the media during Fluo-4 incubation for a total of 40 min before rinsing with Tyrode's solution and imaging (Santos et al., 2019).

For each video, fluorescence intensity of manually selected ROIs (4x4 pixels, in cytoplasm) was measured for each timepoint using Matlab. ROIs were manually excluded if no value exceeded the baseline established in the first 50 s or if spontaneous contractions occurred between 40 and 120 s.

Each transient was evaluated for amplitude (Herington et al., 2015) and time dynamics including response time (Grespan et al., 2016; Halaidych et al., 2019), tau decay constant (Halaidych et al., 2019), and duration (Halaidych et al., 2019; Ahola et al., 2018) by modifying custom Matlab software (Petersen et al., 2018, 2020). Response time is the time between the addition of oxytocin and the maximum fluorescence intensity. Decay is the time between the maximum and 36% of the maximum on the downstroke. Duration spans the time at half of the maximum on the upstroke to the same value on the downstroke. Amplitude is the maximum normalized to the baseline. All ROI results from one coverslip were averaged to represent n=1. Each condition includes coverslips from different experimental batches and days. All data was evaluated with one-way or two-way ANOVA and Tukey's multiple comparisons test in Graphpad Prism.

2.5. Gene expression analysis

Cells from different experimental batches were lysed and RNA was isolated using Qiagen miRNeasy Micro kits per the manufacturer's protocol. Briefly, chloroform was added to cell-Qiazol homogenate for phase separation. The upper aqueous phase was mixed with ethanol, then repeatedly filtered through a spin column with buffer solution and diluted ethanol. RNA was passed through an additional cleaning step (Zymo RNA Clean and Concentrator) then eluted with RNase-free water before storing at $-80\,°C$ prior to sequencing with an Illumina NovaSeq 6000 (performed by Novogene Corporation, Inc.).

Analyses were performed using Partek Flow Genomic Analysis software. Sequenced reads were trimmed from both ends based on a Phred quality score of 20 and a minimum read length of 25 remaining bases then aligned with the STAR algorithm to the hg38 genome. Data was filtered and normalized with the median ratio, then differentially expressed genes were identified with DESeq as p-value <0.01 and fold change greater than the absolute value of 2. Likely due to sample-to-sample variability, we did not observe genes with statistically significant FDR. RNA-seq data were submitted to the National Center for Biotechnology Information (NCBI) Gene Expression Omnibus (GEO) data repository (accession number GSE233288; n = 8 isotropic 13 kPa, n = 8 aligned 13 kPa, n = 8 isotropic 90 kPa, n = 8 aligned 90 kPa).

3. Results

3.1. Engineering models of healthy and fibrotic human myometrium

In a healthy uterus, myometrial tissue is aligned and relatively compliant, with an elastic modulus of approximately 10–30 kPa (Omari et al., 2015; Acar et al., 2016). Fibrotic myometrial tissue is less organized and stiffer, with a two to four-fold increase in tissue stiffness (Acar et al., 2016; Jayes et al., 2019). To determine the effects of fibrotic remodeling on myometrial structure and function, we used our previously established techniques (Ariyasinghe et al., 2017; McCain et al., 2012) to engineer polyacrylamide hydrogels with elastic moduli of 13 kPa and 90 kPa. We then microcontact printed fibronectin onto these hydrogels as a uniform coating or as 40 µm-wide lanes separated by 75 µm gaps (Fig. 1A). Next, we seeded primary human myometrial smooth muscle cells on the hydrogels, cultured them for two days, and stained for nuclei, actin filaments, and fibronectin (Fig. 1B). The number of nuclei per field of view normalized to fibronectin area was not statistically different between conditions (Fig. 1C), indicating consistent cell adhesion and viability. Nuclei aspect ratio was significantly higher in aligned tissues compared to isotropic tissues on 13 kPa hydrogels. Nuclei aspect ratio trended higher in aligned tissues compared to isotropic tissues on 90 kPa hydrogels but did not reach statistical significance (Fig. 1D). The coherency of actin filaments, which ranges from zero for disordered systems to one for oriented or coherent systems, was significantly higher in aligned tissues compared to their isotropic counterparts (Fig. 1E), as expected. Together, these data demonstrate that we can reproducibly engineer human myometrial tissues with independent control over tissue alignment and matrix elasticity to model aspects of healthy and fibrotic tissue.

3.2. Calcium transients in response to oxytocin

Because increased intracellular calcium concentrations are correlated with increased contractile activity in muscle cells (Hill-Eubanks et al., 2011), we next developed a microscopy-based workflow to measure calcium activity in engineered myometrial tissues in response to oxytocin stimulation as a proxy for contractile activity. Our first goal was to establish an oxytocin dose response. To do so, we incubated aligned myometrial tissues on 13 kPa substrates with the fluorescent calcium indicator Fluo-4. We then captured images of Fluo-4 fluorescence for 50 s (rate: 2 frames per second) as a baseline (Fig. 2A). We then added oxytocin at doses ranging from 10^{-4} g/L to 10^{-1} g/L, similar to the range of concentrations used clinically (Uvnäs-Moberg et al., 2019) or in previous *in vitro* studies (Burghardt et al., 1999). We then continued acquisitions for a total of 3 min, which was sufficient for capturing maximum Fluo-4 intensity and return to baseline (Fig. 2A). Next, we processed image stacks with custom Matlab software to produce graphical representations of Fluo-4 intensity over time in multiple regions of interest per field of view and measured the average amplitude, response time, decay, and duration of the resulting calcium transients (Fig. 2B). As expected (Burghardt et al., 1999; Kim et al., 2019), increasing the concentration of oxytocin resulted in calcium transients with faster response time (Fig. 2C), faster decay (Fig. 2D), and shorter duration (Fig. 2E). Amplitude also trended higher as oxytocin increased (Fig. 2F), but without statistical significance. Together, these data demonstrate that calcium transients in our engineered myometrial tissues were responsive to oxytocin in a manner that trended with increasing dosage, which is the expected physiological response.
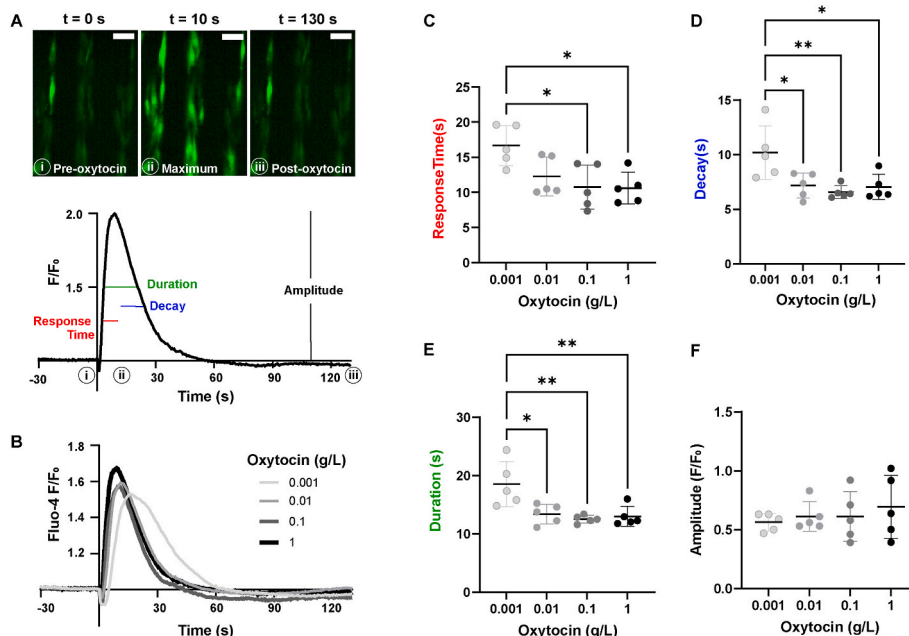
Fig. 2. Calcium transients in response to increasing concentrations of oxytocin. (A) Representative images of baseline (t = 0 s), maximum (t = 10 s), and steady state (t = 130 s) fluorescence intensity. (B) Average calcium transients. (C) Response time, (D) decay, (E) duration, and (F) amplitude dose responses to oxytocin. * denotes $p < 0.05$, ** $p < 0.01$ using Tukey's multiple comparisons test.

3.3. Modulation of calcium transients by tissue alignment and matrix rigidity

To investigate the impact of tissue alignment and matrix rigidity on myometrial physiology, we engineered the four types of tissues shown in Fig. 1 by independently modifying substrate elastic modulus (13 kPa, 90 kPa) and cell alignment. We then performed the same calcium imaging protocol shown in Fig. 2 with 10^{-1} g/L oxytocin since this concentration induced a robust response (Fig. 3A). We proceeded to quantify the same

metrics shown in Fig. 2 and compared all conditions independently with one-way ANOVA. As shown in Fig. 3B, response time was slower in aligned tissues compared to isotropic tissues on 90 kPa substrates. Additionally, aligned tissues on 13 kPa substrates (the closest mimic to healthy tissue) had a longer decay (Fig. 3C) and a longer duration (Fig. 3D) compared to isotropic tissues on 90 kPa substrates (the closest mimic to fibrotic tissue). No significant differences in amplitude were detected (Fig. 3E). We then performed a two-way ANOVA to detect any differences in calcium transients when grouping tissues solely by elastic
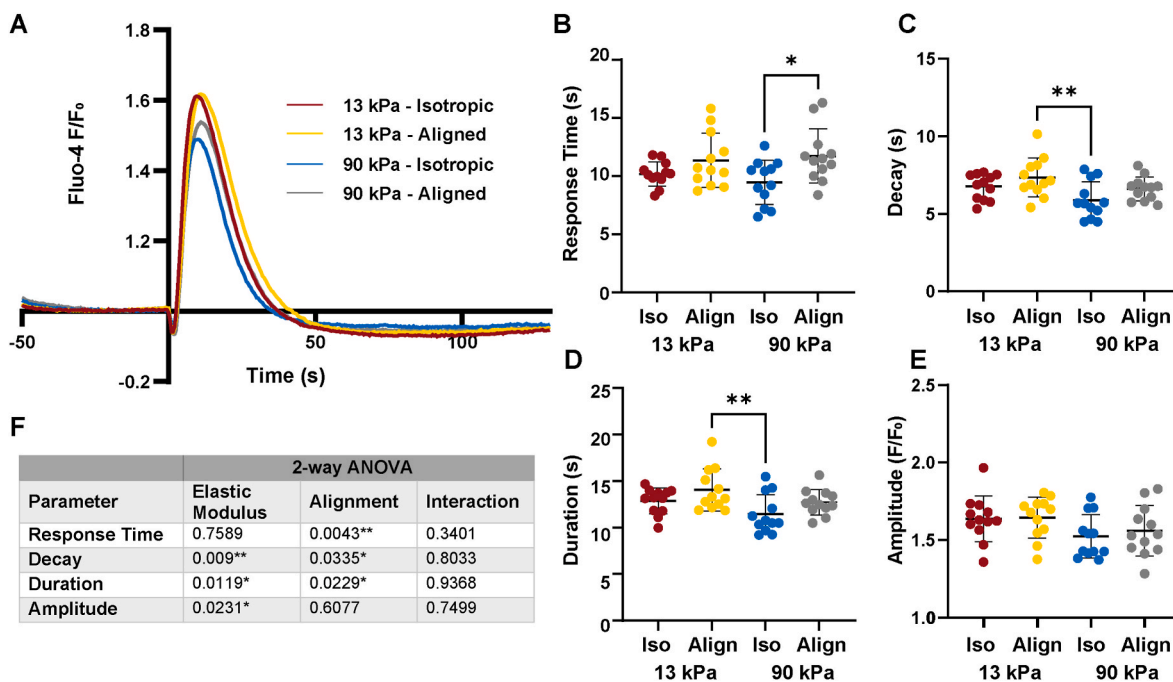
Fig. 3. Calcium transients in engineered myometrial tissues. (A) Average calcium transients for each of the four conditions. (B) Response time, (C) decay, (D) duration, and (E) amplitude at maximum. * denotes $p < 0.05$, ** $p < 0.01$ using Tukey's multiple comparisons test. (F) Two-way ANOVA analysis of calcium transient response to oxytocin as a function of elastic modulus and alignment. * denotes $p < 0.05$, ** $p < 0.01$.

modulus or alignment (Fig. 3F). Interestingly, aligned tissues (independent of elastic modulus) had significantly longer response time, decay, and duration compared to isotropic tissues. Tissues on 13 kPa gels (independent of alignment) had significantly higher amplitude and longer decay and duration. Together, these data suggest that fibrotic myometrial tissues may have a weaker calcium response to oxytocin compared to healthy uterine tissues due to remodeling of tissue architecture and stiffness.

3.4. Modulation of gene expression by tissue alignment and matrix rigidity

To evaluate transcriptional changes based on tissue alignment and matrix rigidity, we performed bulk RNA sequencing on myometrial cells
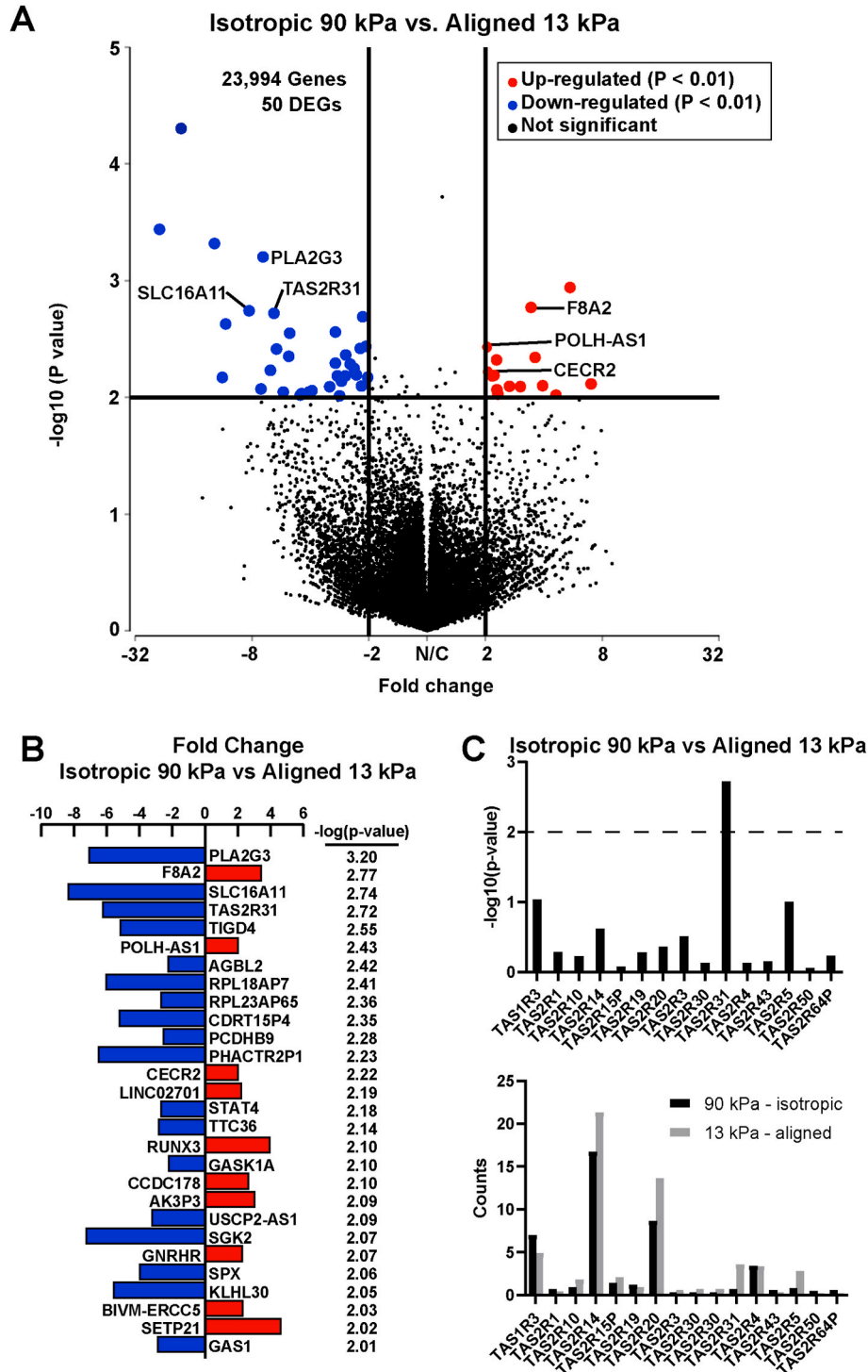

Fig. 4. Transcriptomic analysis of engineered myometrial tissue (A) Volcano plot of comparison between Isotropic 90 kPa and Aligned 13 kPa with down-regulated (blue) and up-regulated (red) genes [$P < 0.01$, absolute value of the fold change (|fold change|>2)]. The dotted black horizontal and vertical lines identify the fold change and p-value cut offs. The DEGs are labeled by gene symbol. (B) Bar graph of fold change for significantly up or downregulated genes. (C) Bar graphs of p-value and normalized gene counts for genes encoding taste receptors. (For interpretation of the references to colour in this figure legend, the reader is referred to the Web version of this article.)

cultured under the same conditions (13 kPa or 90 kPa hydrogels; isotropic or aligned). We compared our stiff and isotropic (90 kPa isotropic) condition (representing fibrotic tissue) to our softer and aligned (13 kPa aligned) condition (representing the healthy tissue) as a volcano plot (Fig. 4A). From this plot, we listed and queried the differentially expressed genes with p-value <0.01 and fold change greater than 2 or less than −2 (Fig. 4B). One of the top differentially expressed genes is *TAS2R31*, which encodes for a bitter taste receptor that is associated with airway (Deshpande et al., 2010) and uterine smooth muscle relaxation (Luo et al., 2019) and thus has been proposed as a target for tocolytics (Zheng et al., 2017). We further mined our data to determine if other bitter taste receptors (TAS2R) are expressed in our engineered tissues. We ultimately detected expression of fourteen other type 2 taste receptors and one type 1 receptor in our healthy- and fibrotic-like tissues (Fig. 4C), consistent with other reports demonstrating that bitter taste receptors are expressed by myometrial smooth muscle cells (Zheng et al., 2017).

3.5. Engineered myometrial tissues mimic clinical responses to compounds

Next, we asked if our engineered tissues would respond as expected to a variety of compounds known to impact the response of myometrial cells to oxytocin. For these experiments, we used aligned myometrial cells on 13 kPa substrates to most closely represent healthy tissues. We also used a relatively low dose of oxytocin (10^{-4} g/L) to ensure a measurable range of responses. First, we tested the impact of pretreating tissues with progesterone. Progesterone is a steroid hormone that maintains the uterus in a quiescent state throughout pregnancy

(Norwitz and Caughey, 2011). Synthetic progesterone is also used as a long-term tocolytic and has been shown to reduce contractility through both non-genomic and genomic mechanisms (Arrowsmith et al., 2010), such as reducing calcium entry (Arrowsmith et al., 2010; Fomin et al., 1999) and modulating oxytocin receptor density (Fomin et al., 1999), respectively. For these reasons, we incubated tissues with progesterone for 24–36 h prior to functional testing to account for any transcriptional changes (Fig. 5A). Progesterone significantly slowed the initial response to oxytocin (Fig. 5B), shortened the decay time to baseline (Fig. 5C), and shortened the overall duration (Fig. 5D), consistent with a dampened contractile response. Although not significant, the amplitude of progesterone-treated tissues trended lower than control, also suggesting a dampened contractile response (Fig. 5E).

Next, we tested the short-term effects of compounds that have previously shown to acutely impact the myometrium. Similar to progesterone, caffeine has a relaxant effect on uterine smooth muscle (Burghardt et al., 1999). Conversely, the coagulation factor thrombin has been associated with preterm labor, likely through direct activation of myosin (Nishimura et al., 2020). Nifedipine is an acute tocolytic sometimes used to quell contractions in the short-term (Arrowsmith et al., 2010). To test the effects of caffeine and thrombin, we added caffeine or thrombin to Tyrode's solution, for a total of 15 min incubation time before imaging. Nifedipine was added at the start of Fluo-4 incubation for a total of 40 min before imaging to align with previous studies (Santos et al., 2019) (Fig. 5A). Caffeine-treated tissues exhibited shorter decay time and shorter duration, similar to progesterone. Response time was slightly delayed by caffeine, but this was not statistically significant. Nifedipine delayed response time but did not affect
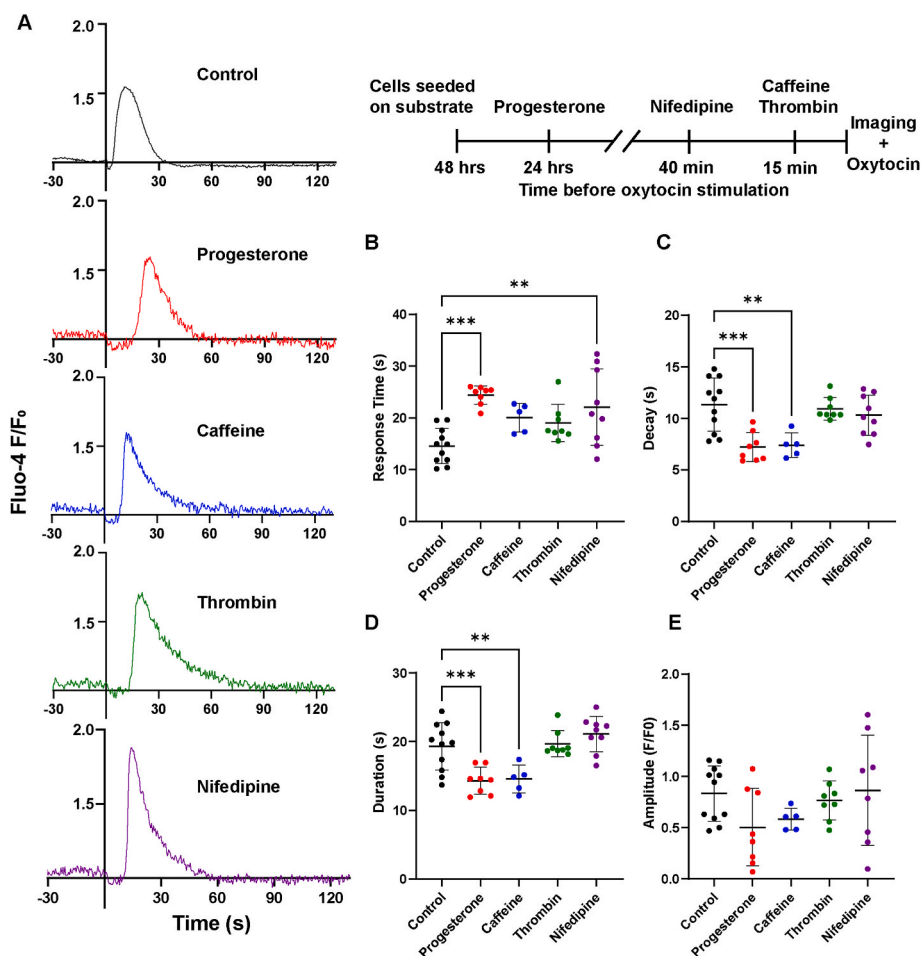
Fig. 5. Compound screening in engineered myometrial tissues. (A) Representative traces of compounds used for screening and timeline of drug addition. (B) Response time, (C) decay, (D) duration, and (E) amplitude at maximum. * denotes p < 0.05, ** p < 0.01, *** p <0.001 using Dunnet's multiple comparisons test.

any other parameters. Thrombin did not cause any effects, suggesting this compound does not impact calcium handling in myometrial smooth muscle cells. Together, these results demonstrate that this platform has potential applications in evaluating the efficacy and mechanisms of actions of new and existing compounds for modulating myometrial smooth muscle physiology.

4. Discussion

Unlike most other muscle tissues, the impact of fibrotic remodeling on myometrial smooth muscle tissue is poorly understood. To address this, we engineered a human *in vitro* model of healthy and fibrotic myometrium by culturing primary human myometrial smooth muscle cells on substrates with independently tunable matrix rigidity and cell alignment. We then characterized tissue structure, oxytocin-induced calcium transients, and the transcriptome, revealing structural, physiological, and genetic changes, respectively, caused by physical features of the tissue microenvironment. In addition, we show that our engineered myometrial tissues respond to select clinical compounds, demonstrating potential applications in drug screening.

To recreate features of the tissue microenvironment characteristic of healthy (Omari et al., 2015; Acar et al., 2016) and fibrotic (Acar et al., 2016; Jayes et al., 2019) myometrium, we cultured primary myometrial smooth muscle cells on polyacrylamide hydrogels with elastic moduli of 13 kPa or 90 kPa that were then microcontact printed with fibronectin as a uniform or lane pattern. One benefit of this approach is that matrix rigidity and tissue alignment can be independently tuned, enabling their effects to be decoupled. We then seeded these substrates with human primary smooth muscle cells isolated from the myometrium. Similar to other muscle cell types (Lyra-Leite et al., 2017; Alford et al., 2011), actin alignment increased on microcontact printed lanes of fibronectin compared to isotropic fibronectin. The circularity of nuclei in isotropic cells also trended lower compared to aligned cells on both 13 kPa and 90 kPa gels, which is consistent with histological data reporting that nuclei in late-stage fibroids become rounded to ovoid (Flake et al., 2013). However, one limitation of our study is that we used purified fibronectin as the only cell adhesion protein, which does not reflect the complex composition of the extracellular matrix in healthy and fibrotic myometrium (Jamaluddin et al., 2018). Myometrial extracellular matrix also comprises laminin and collagen and increased deposition of matrix proteins is a hallmark of fibroids (Winter et al., 2020). Thus, future studies could evaluate matrix protein production as well as the response of myometrial cells cultured on different matrix proteins.

We next performed calcium imaging in response to oxytocin stimulation. We selected oxytocin as our contractile agonist because it has previously been used for clinical (Luca et al., 2020) and *in vitro* (Arrowsmith et al., 2010) applications and induces stronger responses compared to alternative compounds, such as prostaglandins (Balki et al., 2012). With increasing doses of oxytocin, both the response time and decay time of calcium transients declined and thus the overall duration was shorter at higher doses of oxytocin, suggestive of faster release and uptake of intracellular calcium. Calcium transient amplitude also trended upwards with increasing oxytocin concentration, indicative of greater increases in intracellular calcium. Thus, our engineered myometrial tissues retained sensitivity to oxytocin.

To evaluate the impact of fibrotic remodeling on calcium handling, we evaluated calcium transients in engineered myometrial tissues as a function of substrate elastic modulus and tissue alignment. The duration and amplitude of calcium transients were generally highest in aligned tissues on 13 kPa gels and lowest in isotropic tissues on 90 kPa gels, which are the closest mimics of healthy and fibrotic tissues, respectively. These data suggest that fibrotic-like tissues have slower and weaker increases in intracellular calcium in response to oxytocin. To deconvolve the effects of elastic modulus and tissue alignment, we also compared calcium transient metrics using two-way ANOVA. Interestingly, aligned tissues had higher response and decay times (and thus longer durations)

compared to isotropic tissues. However, tissue alignment had no impact on calcium transient amplitude. By contrast, tissues on 13 kPa gels had significantly higher calcium transient amplitude compared to those on 90 kPa gels. Tissues on 13 kPa gels also had higher decay time but no difference in response time. Thus, tissue alignment and matrix rigidity had somewhat distinct impacts on calcium transient morphology.

In myometrial smooth muscle cells, calcium can enter the cytosol via L-type channels on the plasma membrane or via release from internal sarcoplasmic reticulum stores (Pehlivanoğlu et al., 2013). Identifying which calcium pathways and ion channels are sensitive to distinct cues in the tissue microenvironment is an important topic for further investigation to establish the mechanistic underpinnings of our data. Additionally, due to their fundamental role in mechanotransduction, the cytoskeleton or cytoskeletal mediators may link matrix remodeling to changes in myometrial physiology. For example, RhoA has been shown to be more active in leiomyoma cells cultured on rigid polystyrene compared to myometrial cells (Norian et al., 2012). RhoA inhibits myosin light chain phosphatase, which enhances myometrial contractility (Harrod et al., 2011).

To identify differentially expressed genes due to fibrotic-like tissue remodeling, we performed bulk RNA sequencing on our tissue constructs. Because their calcium transients showed the starkest differences, we focused on comparing 13 kPa, aligned tissues to 90 kPa, isotropic tissues. This comparison revealed a relatively small number of differentially expressed genes, none of which were directly related to calcium handling. Thus, the changes we observed in calcium handling were likely not caused by changes in calcium handling proteins at the transcriptional level. In our dataset, the top differentially expressed gene was *PLA2G3,* which encodes for phospholipase A2 group III and was down-regulated in our fibrotic-like tissue compared to the healthy-like tissue. This enzyme hydrolyzes extracellular phospholipids and has been detected in vascular smooth muscle cells (Sato et al., 2008). *SLC16A11,* which encodes for solute carrier family 16 member 11, was also down-regulated in our fibrotic-like tissues and is also involved in lipid metabolism. Thus, remodeling of the tissue microenvironment may be triggering changes in metabolism, which can also impact contractility.

The gene for *TAS2R31* was also downregulated in our fibrotic-like condition. This gene encodes for taste receptor, type 2, member 31, (TAS2R31) which is a bitter taste receptor. Bitter taste receptors (TAS2R) were initially thought to only exist on the tongue, but have also been detected in airway smooth muscle cells. Although the impact of bitter agonists on intracellular calcium in airway smooth muscle cells is variable (Deshpande et al., 2010; Zhang et al., 2013), cells reliably exhibit relaxation or bronchodilation in response to bitter taste receptor agonists. TAS2R receptors have also been detected in uterine smooth muscle cells (Luo et al., 2019). Consistent with these findings, we also detected the expression of fourteen TAS2R and one type 1 receptor (TAS1R) in our tissues. Bitter agonists of TAS2R (e.g., caffeine (Tuzim and Korolczuk, 2021)) have been shown to reverse induced contractions (Zheng et al., 2017) and thus have been proposed as potential targets for a new class of tocolytics. However, if TAS2R expression is down-regulated in fibrotic tissues, TAS2R agonists may have reduced tocolytic effects in these tissues. Thus, identifying if drug targets are modulated by the tissue microenvironment is an important consideration.

We also used our healthy-like tissues (13 kPa, aligned) to test responses to a variety of compounds. As expected, cells incubated with progesterone responded more slowly to oxytocin and decayed more rapidly to baseline, likely because progesterone decreased calcium entry. Similarly, caffeine resulted in a slower response to oxytocin, likely by inhibiting an increase in cAMP (Wray and Prendergast, 2019), which is a mechanism unique to smooth muscle cells. Thrombin has been shown to induce *in vitro* contractions of the myometrium, though it is likely through direct activation of myosin (Nishimura et al., 2020). Thus, it follows that we did not see changes in calcium activity since this

is upstream of the contractile filaments. Nifedipine, a common tocolytic, delayed the start of contraction, but the morphology of the transients did not change. Our results from this panel of compounds demonstrates that we can identify unique effects of compounds on different aspects of calcium handling, which is important for understanding mechanisms of action of new and existing tocolytics or other categories of drugs for myometrial disorders.

In summary, we found that the tissue microenvironment can impact calcium handling in myometrial smooth muscle cells. Our functional model can be used to identify new therapeutic targets (such as bitter taste receptors) and also help identify biomarkers to predict patients who may be at higher risk for adverse labor events. Our study is limited by the inclusion of only one line of human primary myometrial smooth muscle cells. Future studies should evaluate cells from multiple patients, including those with diverse demographic backgrounds or harboring genetic mutations associated with pre-term labor or other conditions. Additionally, our engineered myometrial tissues could be integrated with other Organ on Chip models of the female reproductive system, including those that have focused on the endometrium (Gnecco et al., 2017), placenta (Pemathilaka et al., 2019), and ovaries (Aziz et al., 2020) to evaluate cross-talk with other organs and gain a more comprehensive understanding of female reproductive physiology and pathophysiology.

CRediT authorship contribution statement

Antonina P. Maxey: Conceptualization, Formal analysis, Investigation, Methodology, Software, Visualization, Writing – original draft, Writing – review & editing. **Jaya M. Travis:** Investigation, Software. **Megan L. McCain:** Conceptualization, Funding acquisition, Methodology, Resources, Supervision, Visualization, Writing – original draft, Writing – review & editing.

Declaration of competing interest

The authors declare that they have no known competing financial interests or personal relationships that could have appeared to influence the work reported in this paper.

Data availability

Data will be made available on request.

Acknowledgements

References

Acar, S., Millar, E., Mitkova, M., Mitkov, V., 2016. Value of ultrasound shear wave elastography in the diagnosis of adenomyosis. Ultrasound 24 (4), 205–213. https://doi.org/10.1177/1742271X16673677.

Ahola, A., Pölönen, R.P., Aalto-Setälä, K., Hyttinen, J., 2018. Simultaneous measurement of contraction and calcium transients in stem cell derived cardiomyocytes. Ann. Biomed. Eng. 46 (1), 148–158. https://doi.org/10.1007/s10439-017-1933-2.

Alford, P.W., Nesmith, A.P., Seyward, J.N., Grosberg, A., Parker, K.K., 2011. Vascular smooth muscle contractility depends on cell shape. Integr. Biol. 3 (11), 1063–1070. https://doi.org/10.1039/c1ib00061f.

Ariyasinghe, N.R., Reck, C.H., Viscio, A.A., et al., 2017. Engineering Micromyocardium to Delineate Cellular and Extracellular Regulation of Myocardial Tissue Contractility. https://doi.org/10.1039/c7ib00081b.

Arrowsmith, S., Kendrick, A., Wray, S., 2010. Drugs acting on the pregnant uterus. Obstet. Gynaecol. Reprod. Med. 20 (8), 241–247. https://doi.org/10.1016/j.ogrm.2010.05.001.

Arrowsmith, S., Keov, P., Muttenthaler, M., Gruber, C.W., 2018. Contractility measurements of human uterine smooth muscle to aid drug development. J. Vis. Exp. 131. https://doi.org/10.3791/56639, 01.

Aziz, A.U.R., Yu, X., Jiang, Q., et al., 2020. Doxorubicin-induced toxicity to 3D-cultured rat ovarian follicles on a microfluidic chip. Toxicol. Vitro 62, 104677. https://doi.org/10.1016/j.tiv.2019.104677.

Balki, M., Kanwal, N., Erik-Soussi, M., Kingdom, J., Carvalho, J.C., 2012. Contractile efficacy of various prostaglandins in pregnant rat myometrium pretreated with oxytocin. Reprod. Sci. 19 (9), 968–975. https://doi.org/10.1177/1933719112438971.

Burghardt, R.C., Barhoumi, R., Sanborn, B.M., Andersen, J., 1999. Oxytocin-induced Ca2 + responses in human myometrial cells. Biol. Reprod. 60 (4), 777–782. https://doi.org/10.1095/biolreprod60.4.777.

Desai, R.A., Rodriguez, N.M., Chen, C.S., 2014. "Stamp-off" to micropattern sparse, multicomponent features. Methods Cell Biol. 119, 3–16. https://doi.org/10.1016/B978-0-12-416742-1.00001-9.

Deshpande, D.A., Wang, W.C., McIlmoyle, E.L., et al., 2010. Bitter taste receptors on airway smooth muscle bronchodilate by localized calcium signaling and reverse obstruction. Nat. Med. 16 (11), 1299–1304. https://doi.org/10.1038/nm.2237.

Ewies, A.A.A., Zanetto, U., 2017. Caesarean section scar causes myometrial hypertrophy with subsequent heavy menstrual flow and dysmenorrhoea. Med. Hypotheses 108, 54–56. https://doi.org/10.1016/j.mehy.2017.08.006.

Flake, G.P., Moore, A.B., Sutton, D., et al., 2013. The natural history of uterine leiomyomas: light and electron microscopic studies of fibroid phases, interstitial ischemia, inanosis, and reclamation. Obstet Gynecol Int 2013, 528376. https://doi.org/10.1155/2013/528376.

Flake, G.P., Moore, A.B., Sutton, D., et al., 2018. The life cycle of the uterine fibroid myocyte. Curr Obstet Gynecol Rep 7 (2), 97–105. https://doi.org/10.1007/s13669-018-0241-7.

Fomin, V.P., Cox, B.E., Word, R.A., 1999. Effect of progesterone on intracellular Ca2+ homeostasis in human myometrial smooth muscle cells. Am. J. Physiol. 276 (2), C379–C385. https://doi.org/10.1152/ajpcell.1999.276.2.C379.

Fonck, E., Feigl, G.G., Fasel, J., et al., 2009. Effect of aging on elastin functionality in human cerebral arteries. Stroke 40 (7), 2552–2556. https://doi.org/10.1161/STROKEAHA.108.528091.

Gnecco, J.S., Pensabene, V., Li, D.J., et al., 2017. Compartmentalized culture of perivascular stroma and endothelial cells in a microfluidic model of the human endometrium. Ann. Biomed. Eng. 45 (7), 1758–1769. https://doi.org/10.1007/s10439-017-1797-5.

Grespan, E., Martewicz, S., Serena, E., Le Houerou, V., Rühe, J., Elvassore, N., 2016. Analysis of calcium transients and uniaxial contraction force in single human embryonic stem cell-derived cardiomyocytes on microstructured elastic substrate with spatially controlled surface chemistries. Langmuir 32 (46), 12190–12201. https://doi.org/10.1021/acs.langmuir.6b03138. Nov 22.

Haas, D.M., Benjamin, T., Sawyer, R., Quinney, S.K., 2014. Short-term Tocolytics for Preterm Delivery - Current Perspectives.

Halaidych, O.V., Mummery, C.L., Orlova, V.V., 2019. Quantifying Ca. Biochem. Biophys. Res. Commun. 513 (1), 112–118. https://doi.org/10.1016/j.bbrc.2019.03.143. May 21.

Harrod, J.S., Rada, C.C., Pierce, S.L., England, S.K., Lamping, K.G., 2011. Altered contribution of RhoA/Rho kinase signaling in contractile activity of myometrium in leptin receptor-deficient mice. Am. J. Physiol. Endocrinol. Metab. 301 (2), E362–E369. https://doi.org/10.1152/ajpendo.00696.2010.

Herington, J.L., Swale, D.R., Brown, N., et al., 2015. High-throughput screening of myometrial calcium-mobilization to identify modulators of uterine contractility. PLoS One 10 (11), e0143243. https://doi.org/10.1371/journal.pone.0143243.

Hill-Eubanks, D.C., Werner, M.E., Heppner, T.J., Nelson, M.T., 2011. Calcium signaling in smooth muscle. Cold Spring Harbor Perspect. Biol. 3 (9), a004549. https://doi.org/10.1101/cshperspect.a004549. Sep. 01.

Jamaluddin, M.F.B., Nahar, P., Tanwar, P.S., 2018. Proteomic characterization of the extracellular matrix of human uterine fibroids. Endocrinology 159 (7), 2656–2669. https://doi.org/10.1210/en.2018-00151. Jul 01.

Jayes, F.L., Liu, B., Feng, L., Aviles-Espinoza, N., Leikin, S., Leppert, P.C., 2019. Evidence of biomechanical and collagen heterogeneity in uterine fibroids. PLoS One 14 (4), e0215646. https://doi.org/10.1371/journal.pone.0215646.

Kim, S.H., Riaposova, L., Ahmed, H., et al., 2019. Oxytocin receptor antagonists, atosiban and nolasiban, inhibit prostaglandin F. Sci. Rep. 9 (1), 5792. https://doi.org/10.1038/s41598-019-42181-2. Apr 08.

Lamont, C.D., Jørgensen, J.S., Lamont, R.F., 2016. The safety of tocolytics used for the inhibition of preterm labour. Expet Opin. Drug Saf. 15 (9), 1163–1173. https://doi.org/10.1080/14740338.2016.1187128.

Landman, A.J.E.M., Don, E.E., Vissers, G., et al., 2022. The risk of preterm birth in women with uterine fibroids: a systematic review and meta-analysis. PLoS One 17 (6), e0269478. https://doi.org/10.1371/journal.pone.0269478.

Leppert, P.C., Catherino, W.H., Segars, J.H., 2006. A new hypothesis about the origin of uterine fibroids based on gene expression profiling with microarrays. Am. J. Obstet. Gynecol. 195 (2), 415–420. https://doi.org/10.1016/j.ajog.2005.12.059.

Lou, Z., Huang, Y., Li, S., et al., 2023. Global, regional, and national time trends in incidence, prevalence, years lived with disability for uterine fibroids, 1990-2019: an age-period-cohort analysis for the global burden of disease 2019 study. BMC Publ. Health 23 (1), 916. https://doi.org/10.1186/s12889-023-15765-x. May 19.

Luca, A.M., Carvalho, J.C.A., Ramachandran, N., Balki, M., 2020. The effect of morbid obesity or advanced maternal age on oxytocin-induced myometrial contractions: an

in vitro study. Can. J. Anaesth. 67 (7), 836–846. https://doi.org/10.1007/s12630-020-01615-6, 07.

Luo, M., Ni, K., Jin, Y., Yu, Z., Deng, L., 2019. Toward the identification of extra-oral TAS2R agonists as drug agents for muscle relaxation therapies via bioinformatics-aided screening of bitter compounds in traditional Chinese medicine. Front. Physiol. 10, 861. https://doi.org/10.3389/fphys.2019.00861.

Lyra-Leite, D.M., Andres, A.M., Petersen, A.P., et al., 2017. Mitochondrial function in engineered cardiac tissues is regulated by extracellular matrix elasticity and tissue alignment. Am. J. Physiol. Heart Circ. Physiol. 313 (4), H757–H767. https://doi.org/10.1152/ajpheart.00290.2017.

Marsh, E.E., Al-Hendy, A., Kappus, D., Galitsky, A., Stewart, E.A., Kerolous, M., 2018. Burden, prevalence, and treatment of uterine fibroids: a survey of U.S. Women. J Womens Health (Larchmt) 27 (11), 1359–1367. https://doi.org/10.1089/jwh.2018.7076.

McCain, M.L., Lee, H., Aratyn-Schaus, Y., Kleber, A.G., Parker, K.K., 2012. Cooperative coupling of cell-matrix and cell-cell adhesions in cardiac muscle. Proc. Natl. Acad. Sci. U.S.A. 109 (25), 9881–9886. https://doi.org/10.1073/pnas.1203007109. Jun 19.

Mitchell, B.F., Taggart, M.J., 2009. Are animal models relevant to key aspects of human parturition? Am. J. Physiol. Regul. Integr. Comp. Physiol. 297 (3), R525–R545. https://doi.org/10.1152/ajpregu.00153.2009.

Morse, A., 2022. Stable Fertility Rates 1990-2019 Mask Distinct Variations by Age. United States Census Bureau. Apr 6. https://www.census.gov/library/stories/2022/04/fertility-rates-declined-for-younger-women-increased-for-older-women.html.

Nishimura, F., Mogami, H., Moriuchi, K., Chigusa, Y., Mandai, M., Kondoh, E., 2020. Mechanisms of thrombin-Induced myometrial contractions: potential targets of progesterone. PLoS One 15 (5), e0231944. https://doi.org/10.1371/journal.pone.0231944.

Nishino, M., Togashi, K., Nakai, A., et al., 2005. Uterine contractions evaluated on cine MR imaging in patients with uterine leiomyomas. Eur. J. Radiol. 53 (1), 142–146. https://doi.org/10.1016/j.ejrad.2004.01.009.

Norian, J.M., Owen, C.M., Taboas, J., et al., 2012. Characterization of tissue biomechanics and mechanical signaling in uterine leiomyoma. Matrix Biol. 31 (1), 57–65. https://doi.org/10.1016/j.matbio.2011.09.001.

Norwitz, E.R., Caughey, A.B., 2011. Progesterone supplementation and the prevention of preterm birth. Rev Obstet Gynecol 4 (2), 60–72.

Omari, E.A., Varghese, T., Kliewer, M.A., Harter, J., Hartenbach, E.M., 2015. Dynamic and quasi-static mechanical testing for characterization of the viscoelastic properties of human uterine tissue. J. Biomech. 48 (10), 1730–1736. https://doi.org/10.1016/j.jbiomech.2015.05.013.

Oyelese, Y., Ananth, C.V., 2010. Postpartum hemorrhage: epidemiology, risk factors, and causes. Clin. Obstet. Gynecol. 53 (1), 147–156. https://doi.org/10.1097/GRF.0b013e3181cc406d.

Parazzini, F., Tozzi, L., Bianchi, S., 2016. Pregnancy outcome and uterine fibroids. Best Pract. Res. Clin. Obstet. Gynaecol. 34, 74–84. https://doi.org/10.1016/j.bpobgyn.2015.11.017.

Pehlivanoğlu, B., Bayrak, S., Doğan, M., 2013. A close look at the contraction and relaxation of the myometrium; the role of calcium. J. Turk. Ger. Gynecol. Assoc. 14 (4), 230–234. https://doi.org/10.5152/jtgga.2013.67763.

Pemathilaka, R.L., Caplin, J.D., Aykar, S.S., Montazami, R., Hashemi, N.N., 2019. Placenta-on-a-Chip: in vitro study of caffeine transport across placental barrier using liquid chromatography mass spectrometry. Glob Chall 3 (3), 1800112. https://doi.org/10.1002/gch2.201800112.

Petersen, A.P., Lyra-Leite, D.M., Ariyasinghe, N.R., et al., 2018. Microenvironmental modulation of calcium wave propagation velocity in engineered cardiac tissues. Cell. Mol. Bioeng. 11 (5), 337–352. https://doi.org/10.1007/s12195-018-0522-2.

Petersen, A.P., Cho, N., Lyra-Leite, D.M., et al., 2020. Regulation of calcium dynamics and propagation velocity by tissue microstructure in engineered strands of cardiac tissue. Integr. Biol. 12 (2), 34–46. https://doi.org/10.1093/intbio/zyaa003. Mar 6.

Polio, S.R., Stasiak, S.E., Jamieson, R.R., Balestrini, J.L., Krishnan, R., Parameswaran, H., 2019. Extracellular matrix stiffness regulates human airway smooth muscle contraction by altering the cell-cell coupling. Sci. Rep. 9 (1), 9564. https://doi.org/10.1038/s41598-019-45716-9.

Qin, D., Xia, Y., Whitesides, G.M., 2010. Soft lithography for micro- and nanoscale patterning. Nat. Protoc. 5 (3), 491–502. https://doi.org/10.1038/nprot.2009.234.

Rexius-Hall, M.L., Ariyasinghe, N.R., McCain, M.L., 2021. Engineering shape-controlled microtissues on compliant hydrogels with tunable rigidity and extracellular matrix ligands. Methods Mol. Biol. 2258, 57–72. https://doi.org/10.1007/978-1-0716-1174-6_5.

Rizk, B.R.M.B., Khalaf, Y., Borahay, M.A., 2021. In: Fibroids and Reproduction. CRC Press, Taylor & Francis Group, p. 1 online resource. https://www.taylorfrancis.com/books/9780203728987.

Santos, S., Haslinger, C., Mennet, M., von Mandach, U., Hamburger, M., Simōes-Wüst, A. P., 2019. Bryophyllum pinnatum enhances the inhibitory effect of atosiban and nifedipine on human myometrial contractility: an in vitro study. BMC Compl. Alternative Med. 19 (1), 292. https://doi.org/10.1186/s12906-019-2711-5. Nov 04.

Sato, H., Kato, R., Isogai, Y., et al., 2008. Analyses of group III secreted phospholipase A2 transgenic mice reveal potential participation of this enzyme in plasma lipoprotein modification, macrophage foam cell formation, and atherosclerosis. J. Biol. Chem. 283 (48), 33483–33497. https://doi.org/10.1074/jbc.M804628200. Nov 28.

Simhan, H.N., 2010. Preterm birth is the leading cause of neonatal mortality and is responsible for roughly one-half of long-term neurologic sequelae. Am. J. Obstet. Gynecol. 202 (5), 407–408. https://doi.org/10.1016/j.ajog.2010.03.027.

Souza, G.R., Tseng, H., Gage, J.A., et al., 2017. Magnetically bioprinted human myometrial 3D cell rings as A model for uterine contractility. Int. J. Mol. Sci. 18 (4) https://doi.org/10.3390/ijms18040683.

Spyropoulou, K., Kosmas, I., Tsakiridis, I., et al., 2020. Myomectomy during pregnancy: a systematic review. Eur. J. Obstet. Gynecol. Reprod. Biol. 254, 15–24. https://doi.org/10.1016/j.ejogrb.2020.08.018.

Tuzim, K., Korolczuk, A., 2021. An update on extra-oral bitter taste receptors. J. Transl. Med. 19 (1), 440. https://doi.org/10.1186/s12967-021-03067-y. Oct 21.

Uvnäs-Moberg, K., Ekström-Bergström, A., Berg, M., et al., 2019. Maternal plasma levels of oxytocin during physiological childbirth - a systematic review with implications for uterine contractions and central actions of oxytocin. BMC Pregnancy Childbirth 19 (1), 285. https://doi.org/10.1186/s12884-019-2365-9. Aug 09.

Williams, C., Fong, R., Murray, S.M., Stock, S.J., 2021. Caesarean birth and risk of subsequent preterm birth: a retrospective cohort study. BJOG 128 (6), 1020–1028. https://doi.org/10.1111/1471-0528.16566.

Winter, A., Salamonsen, L.A., Evans, J., 2020. Modelling fibroid pathology: development and manipulation of a myometrial smooth muscle cell macromolecular crowding model to alter extracellular matrix deposition. Mol. Hum. Reprod. 26 (7), 498–509. https://doi.org/10.1093/molehr/gaaa036, 07 01.

Wray, S., Prendergast, C., 2019. The myometrium: from excitation to contractions and labour. Adv. Exp. Med. Biol. 1124, 233–263. https://doi.org/10.1007/978-981-13-5895-1_10.

Zhang, J., Bricker, L., Wray, S., Quenby, S., 2007. Poor uterine contractility in obese women. BJOG 114 (3), 343–348. https://doi.org/10.1111/j.1471-0528.2006.01233.x.

Zhang, C.H., Lifshitz, L.M., Uy, K.F., Ikebe, M., Fogarty, K.E., ZhuGe, R., 2013. The cellular and molecular basis of bitter tastant-induced bronchodilation. PLoS Biol. 11 (3), e1001501 https://doi.org/10.1371/journal.pbio.1001501.

Zheng, K., Lu, P., Delpapa, E., et al., 2017. Bitter taste receptors as targets for tocolytics in preterm labor therapy. Faseb. J. 31 (9), 4037–4052. https://doi.org/10.1096/fj.201601323RR.